Microchimica Acta (2019) 186:830
https://doi.org/10.1007/s00604-019-3960-1

ORIGINAL PAPER

Core-shell hollow spheres of type C@MoS_2 for use in surface-assisted laser desorption/ionization time of flight mass spectrometry of small molecules

Yanfang Zhao[1] · Hanyi Xie[1] · Mei Zhao[1] · Huijuan Li[1] · Xiangfeng Chen[1] · Zongwei Cai[2] · Hexing Song[3]

Received: 3 June 2019 / Accepted: 17 October 2019
© Springer-Verlag GmbH Austria, part of Springer Nature 2019

Abstract

Mesoporous carbon hollow spheres coated with MoS_2 (C@MoS_2) were synthesized to obtain a material with large specific surface area, fast electron transfer efficiency and good water dispersibility. The composite material was applied as a matrix for the analysis of small molecules by surface-assisted laser desorption/ionization time-of-flight mass spectrometry (SALDI-TOF MS). The use of a core-shell C@MoS_2 matrix strongly reduces matrix background interferences and increases signal intensity in the analysis of sulfonamides antibiotics (SAs), cationic dyes, emodin, as well as estrogen and amino acids. The composite material was applied to the SALDI-TOF MS analysis of selected molecules in (spiked) real samples. The ionization mechanism of the core-shell C@MoS_2 as a matrix is discussed. The method exhibits low fragmentation interference, excellent ionization efficiency, high reproducibility and satisfactory salt tolerance.

Keywords Core-shell C@MoS_2 · SALDI-TOF MS · Ionization mechanism · Salt tolerance · Sulfonamides antibiotics · Cationic dyes · Emodin · Estrogen · Amino acids

Introduction

Matrix-assisted laser desorption/ionization time-of-flight mass spectrometry (MALDI-TOF MS) is important in biochemical analysis [1], proteomics [2] and trace analysis [3]. Conventional organic matrices (such as 2,5-dihydroxybenzoic acid (DHB), sinapinic acid (SA), and α-cyano-4-hydroxycinnamic acid, HCCA) do not perform well when applied to analysis of low-molecular-weight compounds (m/z < 500 Da) [4, 5]. To overcome this problem, it is desirable to exploit new organic matrices with low background [6, 7]. Another strategy is to develop inorganic materials which are employed as matrices in surface-assisted laser desorption/ionization mass spectrometry (SALDI MS) [8, 9]. Notably, many inorganic materials such as metal nanoparticles [10, 11], porous silicon [12, 13], metal/metal oxide nanoparticles [14, 15], magnetic nanoparticles [16, 17], quantum dots [11, 18] and inorganic carbon-based materials [19, 20] have been introduced as solid matrices [21]. They can avoid the complication of co-crystallization and background interference, and provide excellent sensitivity [22].

Due to their high specific surface area, excellent conductivity, rapid energy transfer efficiency and good thermal stability, carbon-based nanomaterials have been demonstrated to be an effective matrix for SALDI-TOF experiment [23]. One of major concern for usage of these materials as matrix in SALDI-TOF is their low dispersibility in solution. This limitation may lead to inhomogeneous distribution of nanomaterials on the target plate resulting in poor reproducibility and low sensitivity. Hybridization with nanomaterial having good dispersibility is a practical way to improve the performance of carbon nanomaterial in SALDI-TOF MS experiment. MoS_2 nanosheets have 2D ultrathin graphic like

Electronic supplementary material The online version of this article (https://doi.org/10.1007/s00604-019-3960-1) contains supplementary material, which is available to authorized users.

✉ Xiangfeng Chen
qlgdchenxf@126.com

[1] Key Laboratory for Applied Technology of Sophisticated Analytical Instruments of Shandong Province, Shandong Analysis and Test Centre, Qilu University of Technology (Shandong Academy of Sciences), Jinan 250014, China

[2] State Key Laboratory of Environmental and Biological Analysis, Department of Chemistry, Hong Kong Baptist University, Hong Kong 999077, People's Republic of China

[3] Intelligene Biosystems (QingDao) Co. Ltd., Qingdao 266400, China

Published online: 21 November 2019

structure, and have been great attention in optoelectronics, and energy harvesting [24]. Importantly, MoS_2 nanosheets have strong absorption in the UV visible range, making it possible for SALDI application [25].

We describe a water dispersible core-shell C@MoS_2 composite material that was prepared by in situ growth of MoS2 nanosheets on the surfaces of mesoporous carbon hollow spheres (MCHS). The as-synthesized hybrid materials have hydrophobic inner surface with hydrophilic outer MoS_2 layers, which exhibited good dispersibility, high surface area, and strong absorption in the UV visible range. Herein, the MCHS are embedded into the center part of the MoS_2 shell, to endow the hybrid composite of C@MoS_2 with the great synergistic effect for the laser desorption/ionization. To the best of our knowledge, no attempt has yet been made to synthesize the core-shell structured C@MoS_2 and apply it as the surface assisted material for SALDI-TOF MS in the sensitive detection of small molecules.

Experimental Section

Reagents

(NH4)6Mo7O24·4H2O, thiourea, cationic dyes of methylene blue (MB), new methylene blue (NMB), mountain green (MG), crystal violet (CV) and rhodamine B (Rh B) were bought from Sinopharm Chemical Reagent Co., Ltd. (Shanghai, China, https://www.reagent.com). Standards of sulfacetamide (SA), sulfapyridine (SP), sulfamerazine (SM), sulfadimethoxine (SDM) were purchased from heowns Co., Ltd. (Tianjin, China, http://www.heowns.com). Emodin, estrogens including Bisphenol A (BPA), octylphenol (OP) and nonylphenol (NP) and amino acids including L-phenylalanine(L-Phe), D, L arginine (D, L-Arg), and L-tryptophan(L-Try) were bought from Aladdin (Shanghai, China, http://www.aladdin-e.com). Ultrapure water from a Millipore Milli-Q water purification system was used for experiments.

Instrumentation

Scanning electron microscopy (SEM) photos were measured on a SWPRATM 55 field emission environmental SEM (Carl Zeiss Micro Imaging Co., Ltd., Germany). A JEM-2100 microscope (JEOL, Tokyo, Japan) was used for transmission electron microscopy (TEM). The specific surface area of Brunauer-Emmett-Teller was obtained using an ASAP 2020 porosimeter (Micromeritics, USA). UV-vis spectrum was measured through a multimode microplate reader (TECAN SPARK 20 M, Switzerland). X-ray photoelectron spectroscopy was recorded by Thermo Esca Lab 250Xi spectrometer.

Synthesis procedure

Preparation of C@MoS_2 composite MCHS was synthesized according to reported method [26] in the Electronic Supplementary Material (ESM). The core-shell C@MoS_2 composite was prepared by an in situ growth method. In brief, 0.70 g (NH4)6Mo7O24·4H2O and 4.56 g thiourea were dispersed in 60 mL ultrapure water. A homogeneous solution was attained with bath sonication. Next, 20 mg MCHS was added, and the mixture was transferred into hydrothermal reactor and reacted at 200 °C for 10 h. The precipitate was obtained via centrifugation, washed extensively three times with ultrapure water. Finally, the black product was heated at 70 °C for about 6 h.

Sample preparation

The stock solutions of the sulfonamide antibiotic, emodin and estrogen were prepared at a concentration of 1 μM with methanol. Cationic dyes and amino acids were dissolved in water to obtain the 1 μM stock solutions. All solutions were stored at ~4 °C for further use. The saturated HCCA solution was prepared in 0.1% TFA in water/acetonitrile (15/85, *v*/v). 10 mg·mL^{-1} of DHB was prepared in 0.1% TFA in water/acetonitrile (70/30, v/v). 10 mg·mL^{-1} of Core-shell C@MoS_2 was dispersed in water/methanol (1/1, v/v) and was sonicated for 1 min, then 1 μL of analyte solution was pipetted onto a 384-ground steel plate and dried under ambient conditions to form a thin layer. Then, 1 μL the matrix suspension was pipetted onto the layer of analyte prior to MALDI-TOF MS tests. The strategy was also employed for test of analytes in real samples. The pretreatment procedure of real samples was described in the ESM.

MALDI-TOF-MS analysis

All mass data was recorded by *rapifleX*™ MALDI-TOF-MS (Bruker Daltonics, Germany) and Quan TOF (Intelligent Biosystems, Co. Ltd., Qingdao, China). The MALDI source nitrogen laser was set at 337 nm, the accelerating voltage was set from −20 kV to 20 kV and mass spectra were acquired with 1000 laser shots. The details of instrumental parameters were given in in Table S1.

Results and discussion

Choice of materials

MoS_2 was selected as dopant to improve the performance of MCHS in LDI-TOF MS analysis of small molecules. As shown in Fig. 1(a), a two-step procedure was adopted to synthesis core-shell C@MoS_2 composite. After silica assisted

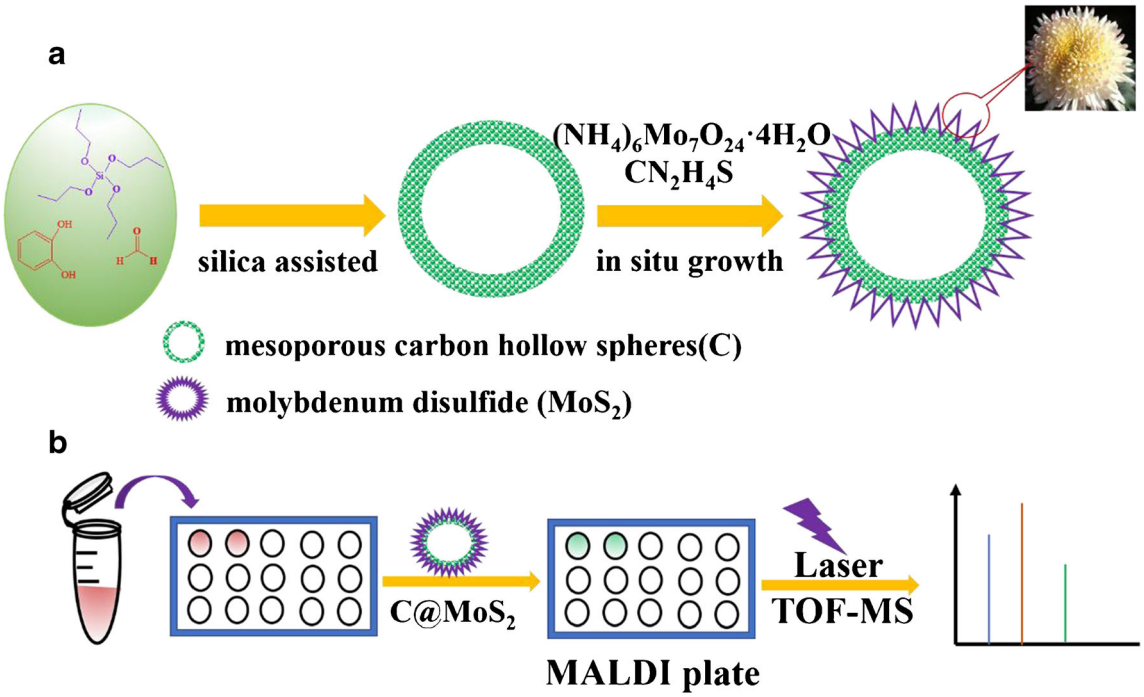

Fig. 1 **a** Schematic diagram of core-shell C@MoS_2; **b** SALDI-TOF MS analysis using core-shell C@MoS_2 as the surface-assisted material

fabrication of MCHS, the MoS_2 was in situ grown on the surface of MCHS. The as-synthesized hybrid materials have hydrophobic inner carbon surface with hydrophilic outer MoS_2 layers. The composite should combine the advantages of good dispersibility, high specific area, and strong absorption in the UV visible range, and overcome the limitations of carbon-based nanomaterials in dispersibility. The flower like composite was used in SALDI-TOF MS analysis of small molecules (Fig. 1b). Antibiotics, cationic dyes, emodin, estrogens and amino acids were used as target analytes.

Characterization of the core-shell C@MoS_2 composite

SEM images of mesoporous monodispersed MCHS are shown in Fig. 2a. An average size of 300 nm was obtained. In the process of material synthesis, the morphology was greatly affected by temperature. Therefore, in order to ensure the uniformity of the material, the temperature should be strictly controlled. The average diameter of core-shell C@MoS_2 composites increased to 330–350 nm (Fig. 2b), thereby demonstrating that MoS_2 was successfully coated on MCHS. TEM was further recorded and is shown in Fig. 2c. Obvious ripples and corrugations appeared on the composite material surface, thereby revealing the successful formation of high crystalline and ultrathin MoS_2 nanosheets. TEM image (Fig. 2d) further verified that the composite material comprised a compact core and a shell (approximately 30–50 nm) with lower density. Figure 2e showed an absorption in the near UV region at about 355 nm of the composites, which made core-shell C@MoS_2 composites a promising matrix in MALDI for absorbing and transferring laser energy to the analytes. Better dispersibility was obtained for core-shell C@MoS_2 composites than pure MCHS from insert Fig. 2e. N_2 adsorption and desorption isotherms were used to characterize the specific surface area (Fig. 2f), which was 568 $m^2 \cdot g^{-1}$. The BJH curve (Fig. 2f insert) showed relatively fixed mesopores with sizes of approximately 3 nm. The core-shell C@MoS_2 composite was further characterized by X-ray photoelectron spectroscopy (XPS) techniques. Fig. S1a, In the C 1 s spectrum, the main peak at 284.7 eV is corresponding to sp2 carbon (C − C or C=C) [26]. From Fig. S1b, the component at 226.0 eV corresponds to S 2 s of MoS2. The two main intense Mo 3d5/2 (228.8 eV) and Mo 3d3/2 (232.1 eV) components are characteristic of MoS2. In XPS S 2p core-level spectrum (Fig. S1c), the main doublet located at binding energies of 161.6 and 162.9 eV corresponds to the S 2p3/2 and S 2p1/2 components of MoS2. The composite was also characterized by energy dispersive spectrum analysis (Fig. S1d), and the atomic ratio between S and Mo was calculated to be 2:0.85.

Applications of the C@MoS_2 in SALDI-TOF MS

Sulfacetamide antibiotics Sulfonamide antibiotics (SAs), with potential hazardous to water and human health, are universally employed in modern humans and animal medical practices [27, 28]. Herein, SAs was used as probe to access the performance of core-shell C@MoS_2 in SALDI-TOF MS. As presented in Fig. S2(a-e), the five SAs were obtained by the assistance of the composite material in positive ion mode.

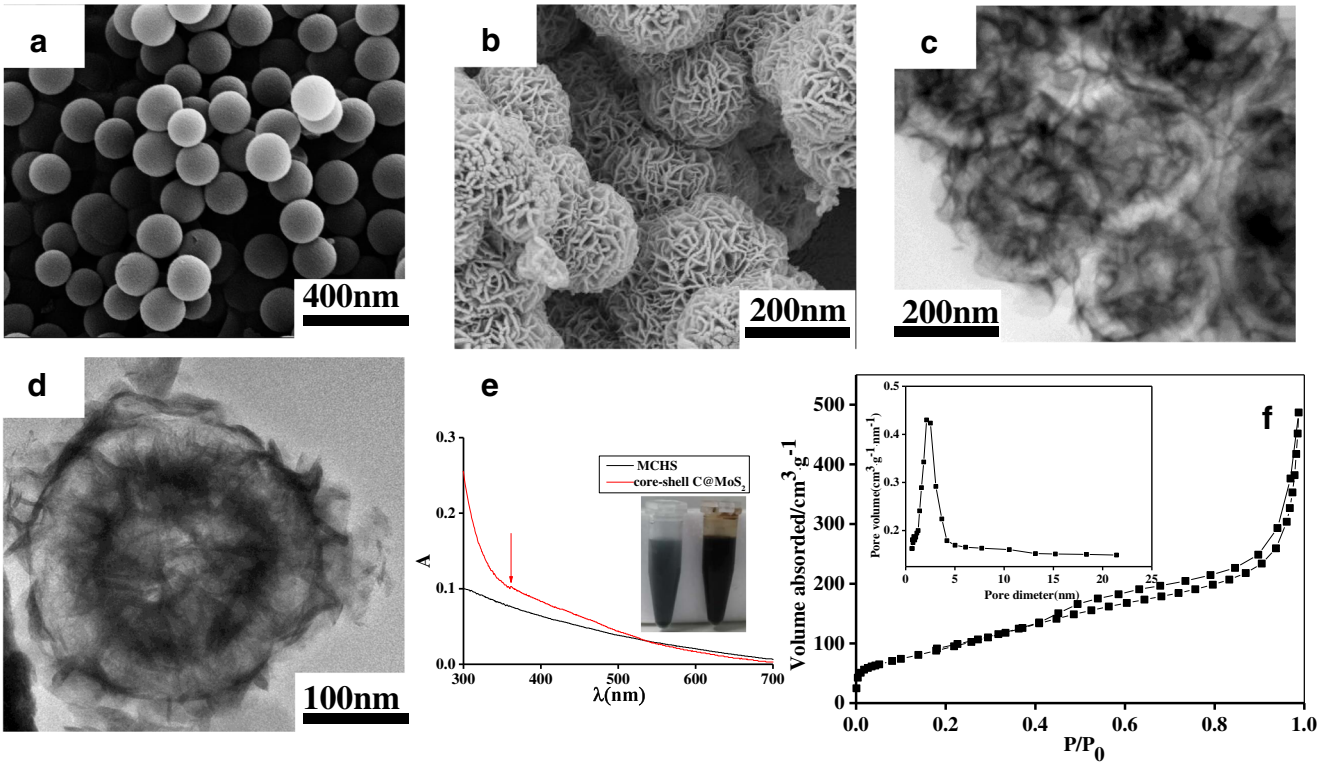

Fig. 2 **a** SEM image of MCHS (a) and core-shell C@MoS_2 **b**, TEM image of core-shell C@MoS_2 **c**; HRTEM image of core-shell C@MoS_2 **d**, UV-vis spectra of MCHS and core-shell C@MoS_2 dispersed in water **e**. Inset in (e) shows the photographs of MCHS (left) and core-shell C@MoS_2 (right) and N_2 adsorption-desorption isotherms **f** and inset in (f) the pore size distributions for core-shell C@MoS_2

The MS peaks were agreement with the protonated ion $[M + H]^+$ (m/z 215.14) for SA, $[M + H]^+$ (m/z 250.08) for SP, $[M + H]^+$ (m/z 265.08) for SM, $[M + H]^+$ (m/z 279.10) for SMZ, and $[M + H]^+$ (m/z 311.09) for SDM. Additionally, the composite material showed a clean background in positive ion mode in Fig. S3a. Less interference was observed in the spectra as compared with those obtained using HCCA (Fig. S3b) towards SAs. To further illustrate the applicability, the SAs were determined in a real sample. As shown in Fig. 3a, no SAs were detected in the milk sample. When the concentration of 1 μM of five SAs mixture was spiked, the signals were detected with a little interfering background in the spectrum (Fig. 3b), clearly demonstrating the application of the method.

Cationic dyes Cationic dyes, such as MB, NMB, MG, CV and RhB, represent an important group of organic compounds, which have a variety of scientific and industrial applications [29]. The core-shell C@MoS_2 was used for SALDI-TOF MS detection of cationic dyes. As presented in Fig. S4(a-e), the five cationic dyes were obtained under the assistance of the core-shell C@MoS_2 in positive ion mode. The MS peaks were agreement with the protonated ion $[MB]^+$ (m/z 284.13), $[NMB]^+$ (m/z 312.17), $[MG]^+$ (m/z 329.21), $[CV]^+$ (m/z 372.25), and $[RhB]^+$ (m/z 433.23). It was noteworthy that the signals response of the five cationic dyes produced by using core-shell C@MoS_2 were much higher than those obtained with DHB. In addition, there was less interference than those obtained using HCCA (Fig. S5). Cationic dyes in a water sample was also analyzed. As shown in Fig. 3c, MB and RhB were detected in waste water samples. Although the MS peaks of the substrate of water sample had slightly influence on the detection of cationic dyes, all the selected cationic dyes were observed in when the water sample was spiked with 1 μM above cationic dyes mixture in Fig. 3d.

Emodin Emodin, as the key component of traditional Chinese medicine [30], (MW = 270.24) was also chosen as model analyte to investigate the performance of C@MoS_2 in SALDI-TOF MS. As presented in Fig. S6, emodin was obtained by the assistance of the core-shell C@MoS_2 in negative ion mode, where the MS peak was agreement with the deprotonated ion $[M-H]^-$(m/z 269.02) for emodin. Clearly, the signal intensity produced using the core-shell C@MoS_2 matrix was higher than those detected by HCCA or DHB matrices (Fig. S7). The method was also applied for analysis of emodin in blank rat plasma (Fig. 4a). When the concentration of 1 μM of emodin was spiked, the signals were detected with a little interfering background in the spectrum. This inferred that the strategy might provide a new promising alternative for rat plasma analysis (Fig. 4b).

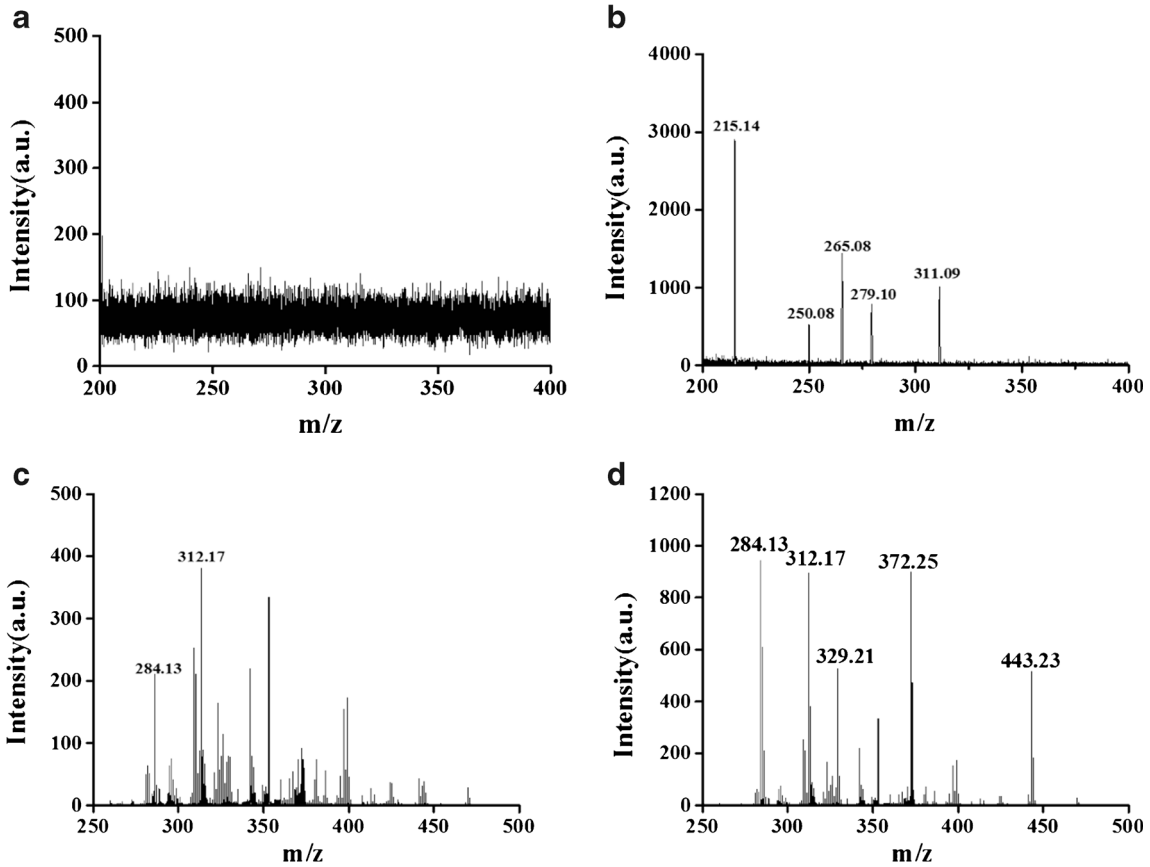

Fig. 3 SALDI-TOF MS analysis of five SAs in blank milk (**a**) and spiked by 1 μM SAs (**b**) in milk, five cationic dyes in water (**c**) and spiked by 1 μM cationic dyes (**d**) in water using the core-shell C@MoS_2 matrix. Positive ion mode. Laser intensity: 60%

Estrogen BPA (MW = 228.29), OP (MW = 206.32) and NP (MW = 220.24) are typical estrogen [31]. As shown in Fig. S8(a-c), under the matrix of the core-shell C@MoS_2 in negative ion mode, the three estrogen samples were obtained remarkably. The MS peaks were agreement with the deprotonated ion $[M\text{-}H]^-$ (m/z 227.23) for BPA, $[M\text{-}H]^-$ (m/z 219.03) for NP, and $[M\text{-}H]^-$ (m/z 205.01) for OP. Compared to HCCA and DHB, a good signal is obtained when using C@MoS_2 as the matrix (Fig. S9). To further prove the analytical performance of core-shell C@MoS_2 as a matrix, we applied core-shell C@MoS_2 for the analysis of a mixture of estrogen in orange juice of buckets, as shown in Fig. 4c. When the concentration of 1 μM of above three mixture was spiked, the signals were detected with a clean background in the spectrum, which clearly offered the application of the strategy (Fig. 4d).

Amino acids The development of sensitive and fast detection strategies towards amino acid is urgent to meet the growing demand of clinical diagnosis [32]. Fig. S10(a-c) showed that all three amino acids were tested obviously with low background interference and characteristic $[M\text{-}H]^-$ ion signals. Three amino acids at m/z 164.09, 173.13 and 203.07 were corresponding to the $[M\text{-}H]^-$ for L-Phe, D, L-Arg, and L-Try respectively. Compared to HCCA and DHB, a good signal is obtained when using C@MoS_2 as the matrix (Fig. S11). Similarly, as shown in Figs. 5a and 6b, when the concentration of 1 μM of above three mixture was spiked, the three amino acids were also detected with the core-shell C@MoS_2 matrix in blank urine.

Reproducibility and salt tolerance

Reproducibility is a commonly encountered problem in conventional MALDI-TOF MS. The MS intensity which was acquired for 10 times of one sample spot. As shown in Fig. 5c and Table 1, the relative standard deviation (RSD) from was 2.13%, 4.42%, 2.28%, 6.65%, 4.41% for SA, RhB, emodin, BPA and L-Phe, respectively. These results suggested a good signal reproducibility. The full width at half maximum (FWHM) and the limits of detection (LOD) were also summarized in Table 1. The FWHM indicated that the core-shell C@MoS_2 matrix was favorable for obtaining high resolution (Table 1). The LOD for selected analytes were estimated, which suggested the high sensitivity of SALDI-TOF MS with the assistance of core-shell C@MoS_2 matrix.

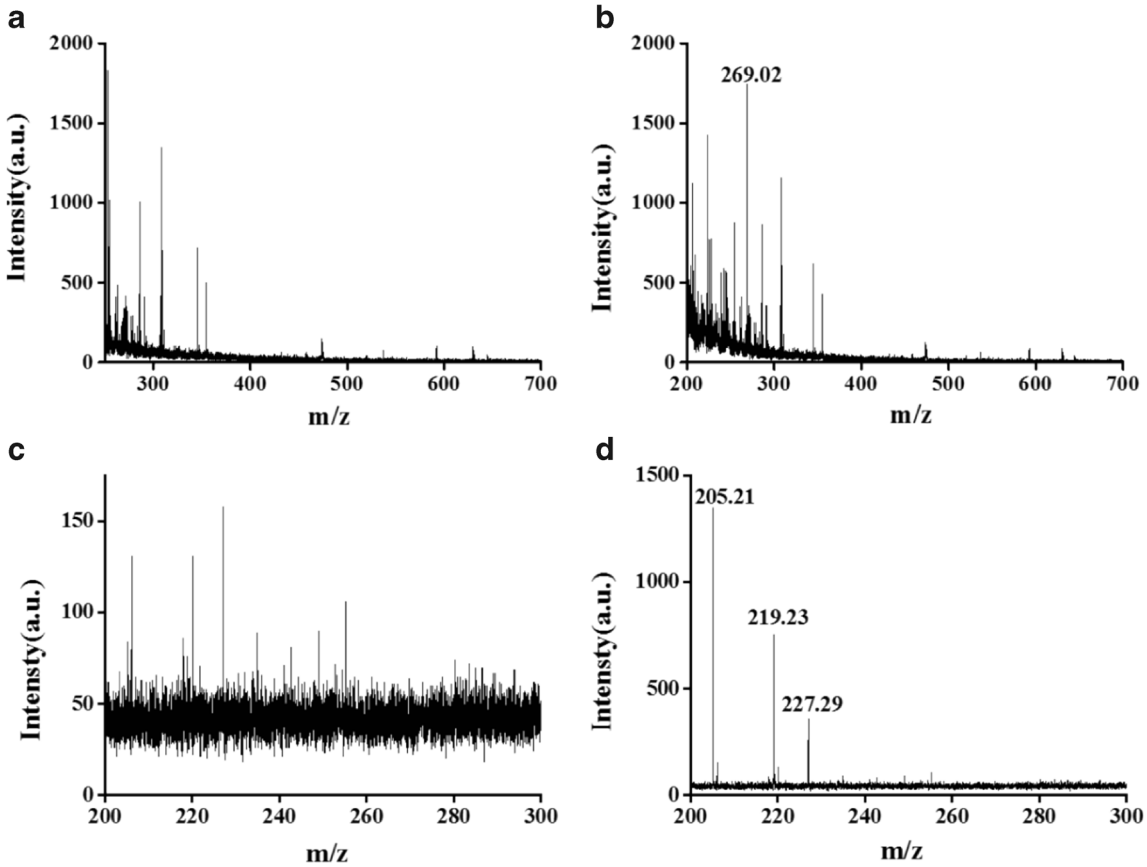

Fig. 4 SALDI-TOF MS analysis of five emodin in blank rat plasma (**a**) and spiked by 1 μM emodin (**b**) in rat plasma, three estrogens in blank orange juice of buckets (**c**) and spiked 1 μM of three estrogens in sample(**d**) using the core-shell C@MoS_2 matrix. Negative ion mode. Laser intensity: 60%

Salt tolerance is vital to evaluate MALDI-TOF MS method. With the mixture of analytes (SAs, cationic dyes, emodin, estrogens and amino acids) added up to 500 mM NaCl, the signals decreased 9.56% (Fig. S12), 9.33% (Fig. S13), 4.57% (Fig. S14), 9.68% (Fig. S15), 9.96% (Fig. S16) for SA, RhB, emodin, BPA and L-Phe, respectively. The phenomenon was suggested a satisfactory salt tolerance of the C@MoS_2 matrix.

Comparison with other solid matrices

The matrix effects of several commercially available materials including graphene, MWCNT and boron nitride (BN) were compared with the core-shell C@MoS_2. As seen in Fig. 6a, three amino acids were chosen as the target analytes, the core-shell C@MoS_2 exhibited the highest ionization efficiency

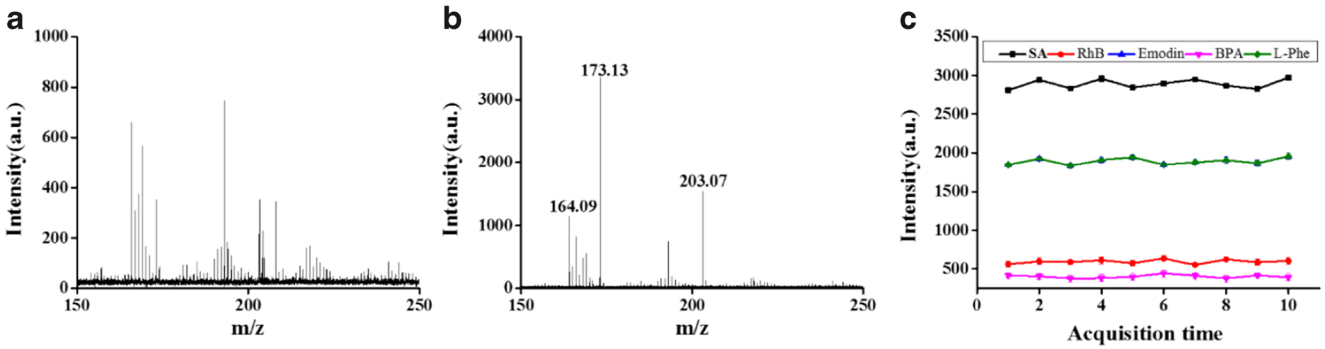

Fig. 5 SALDI-TOF MS analysis of three amino acids in blank urine (**a**) and spiked by 1 μM amino acids in sample (**b**) by the core-shell C@MoS_2 matrix; MS signal intensity of various small molecules (including SA, RhB, Emodin, BPA and L-Phe) by the core-shell C@MoS_2 matrix. Continuous 10 spectra were obtained by applying laser shots on random positions uniformly located on the spot. Each analyte was 1 μM. $n = 10$, Laser intensity: 60%. Negative ion mode. Laser intensity: 60%

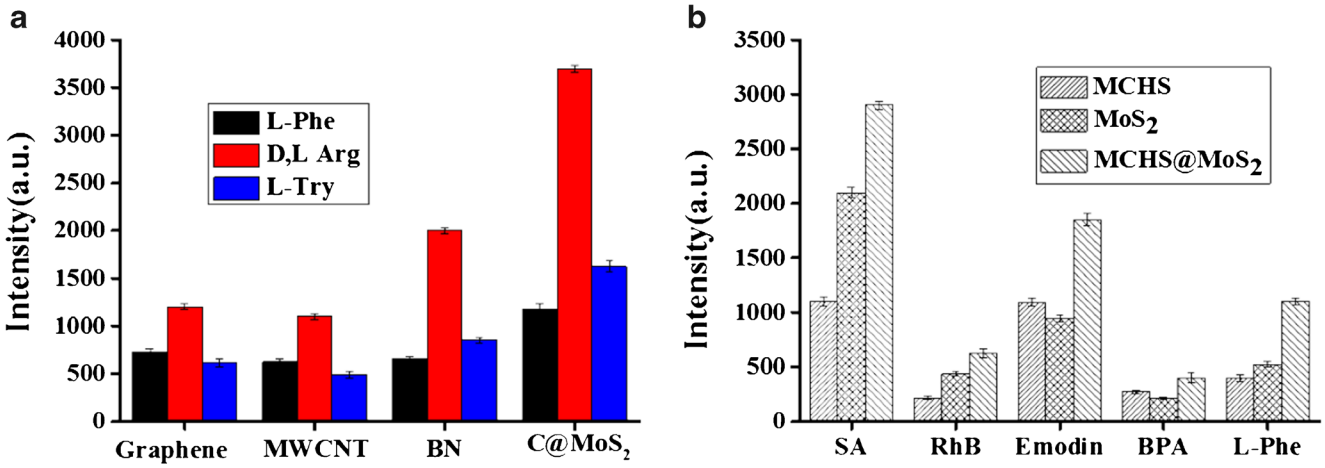

Fig. 6 **a** Comparison of performance of different matrices (graphene, MWCNT, BN, and core-shell C@MoS_2 composites in SALDI-TOF MS detection of L-Phe (black), D, L-Arg(red), and L-Try; **b** Comparison of mass peak intensities of various small molecules (including SA, RhB, Emodin, BPA and L-Phe) with MCHS, MoS_2, and core-shell C@MoS_2 composites as surface-assisted material for SALDI-TOF MS. Analyte concentration: 1 μM

amongst all four matrices. The relative mass peak intensities of small molecules obtained from MCHS, MoS_2, and core-shell C@MoS_2 composites were shown in Fig. 6b, the results showed that the ion intensities of small molecules desorbed from core-shell C@MoS_2 composites were higher than that from MCHS and MoS_2, indicating that the composite was propitious to enhance the desorption/ionization efficiency of small analytes.

Possible ionization mechanism of C@MoS_2 matrix

As shown in Fig. 1, the surface of composite material was coating with nanoflower-like MoS_2, which clearly changed the structure and morphology of MCHS. The MoS_2 makes the matrix become more hydrophilic with good water dispersibility (Fig. 2e). This behavior is beneficial for the homogeneous sample spreading, which increase the shots-to-shot and samples-to-sample reproducibility. The modification of mesoporous carbon hollow spheres (MCHS) inside the MoS_2 nanosheet yields larger surface area for adsorption of analyte. The analytes were firstly trapped and/or concentrated by the composite. The MoS_2 has high adsorption coefficients in the near UV-visible region [25]. In the irradiation step, the composite could therefore effectively adsorb energy from incident light. As a thermo-driven likely process, the energy was then transferred from the matrix material to the analyte, and induced the ionization reaction. The MoS_2 sheet edges have been identified as the active sites to adsorb and dissociate H_2 through hydrogen evolution reaction (HER) [33]. The HER might provide protons for the formation of positive species in SALDI process. The ratio of Mo: S obtained from the EDX spectrum is calculated to be 0.85: 2, which suggest the existence of abundant Mo vacancy. In the negative mode, these vacancy sites may act as proton acceptance site. The hybridization of MoS_2 material not only increases the dispersibility of MCHS, but also enhances the interaction between the analytes and the solid matrix surface. In addition to the non-covalent between the MCHS and analytes, the partial filled d-orbital of the surface Mo atom and π-bond in analytes should also induce the cation-π interaction and partial electron transfer from the analytes to the metal [24]. The stronger interaction is beneficial for the thermal conductivity and electron transport, and thus increases the ionization efficiency of analytes [25]. The mechanism of solid matrix is complex and further efforts are needed to better understand the roles and functions of core-shell C@MoS_2 matrix in SALDI.

Table 1 Analytical parameters of analytes by core-shell C@MoS_2 matrix

Analyte	Characteristic ion (m/z)	Reproducibility RSD,%(n = 10)	FWHM (m/z)	LOD (pmol)
SA	215.14	2.13	0.0135	2
RhB	443.23	4.42	0.0131	8
Emodin	269.02	2.28	0.0176	4
BPA	227.23	6.65	0.0198	10
L-Phe	164.09	4.41	0.0124	6

Conclusion

A core-shell C@MoS_2 composite was adopted as a solid matrix of SALDI-TOF MS of small molecules. The matrix displayed some merits such as good sensitivity and little background interference. Additionally, the results of real sample analyses demonstrated the potential applications of C@MoS_2 for complex samples. It is expected that the core-shell C@MoS_2 used as matrix with SALDI-TOF MS strategy can

be broadened to other types of small molecules detection. Further efforts to understand the mechanism, and the application in other small molecules using the core-shell C@MoS_2 composites should be investigated.

Acknowledgements This work was supported by The National Key Research and Development Program of China (2018YFC1603500), Natural Science Foundation of Shandong Province (ZR2017MB011), Key R&D Program of Shandong Province (2019GSF111009, 2019GSF111001), Key Laboratory of Biomedical Effects of Nanomaterials and Nanosafety, CAS(NSKF201813), the Special Grant for High-Level Overseas Talents of Shandong Academy of Sciences, Youth Science Funds of Shandong Academy of Sciences (2019QN008,2019QN009).

References

1. Reiding KR, Blank D, Kuijper DM, Deelder AM, Wuhrer M (2014) High-throughput profiling of protein N-glycosylation by MALDI-TOF-MS employing linkage-specific sialic acid esterification. Anal Chem 86:5784–5793. https://doi.org/10.1021/ac500335t
2. Chen HM, Deng CH, Zhan XM (2009) Synthesis of Fe_3O_4@SiO_2@PMMA core–shell–shell magnetic microspheres for highly efficient enrichment of peptides and proteins for MALDI-TOF MS analysis. Angew Chem Int Edit 122:617–621. https://doi.org/10.1002/anie.200904885
3. Zhou X, Wei Y, He Q, Boey F, Zhang Q, Zhang H (2010) Reduced graphene oxide films used as matrix of MALDI-TOF-MS for detection of octachlorodibenzo-p-dioxin. Chem Commun 46:6974–6976. https://doi.org/10.1039/c0cc01681k
4. Shi CY, Meng JR, Deng CH (2012) Enrichment and detection of small molecules using magnetic graphene as an adsorbent and a novel matrix of MALDI-TOF-MS. Chem Commun 48:2418–2420. https://doi.org/10.1039/c2cc17696c
5. Min QH, Zhang XX, Chen XQ, Li S, Zhu J-J (2014) N-doped graphene: An alternative carbon-based matrix for highly efficient detection of small molecules by negative ion MALDI-TOF MS. Anal Chem 86:9122–9130. https://doi.org/10.1021/ac501943n
6. Wang YM, Gao D, Chen YL, Hu GN, Liu HX, Jiang YY (2016) Development of N,S-doped carbon dots as a novel matrix for the analysis of small molecules by negative ion MALDI-TOF MS. RSC Adv 6:79043–79049. https://doi.org/10.1039/c6ra12131d
7. Gao C, Zhen DS, He N, An ZB, Zhou QL, Li CY, Grimes CA, Cai QY (2019) Two-dimensional TiO_2 nanoflakes enable rapid SALDI-TOF-MS detection of toxic small molecules (dyes and their metabolites) in complex environments. Talanta 196:1–8. https://doi.org/10.1016/j.talanta.2018.11.104
8. Li XS, Wu JH, Xu LD, Zhao Q, Luo YB, Yuan BF, Feng YQ (2011) A magnetite/oxidized carbon nanotube composite used as an adsorbent and a matrix of MALDI-TOF-MS for the determination of Benzo[a]pyrene. Chem Commun 47:9816–9818. https://doi.org/10.1039/c1cc13166d
9. Liu Q, Cheng MT, Wang J, Jiang GB (2015) Graphene oxide nanoribbons: improved synthesis and application in MALDI mass spectrometry. Chem-Eur J 21:5594–5599. https://doi.org/10.1002/chem.201406280
10. Sangsuwan A, Narupai B, Sae-ung P, Rodtamai S, Rodthongkum N, Hoven VP (2015) Patterned poly(acrylic acid) brushes containing gold nanoparticles for peptide detection by surface-assisted laser desorption/ionization mass spectrometry. Anal Chem 87:10738–10746. https://doi.org/10.1021/acs.analchem.5b00734
11. Abdelhamid HN (2018) Nanoparticle assisted laser desorption/ionization mass spectrometry for small molecule analytes. Microchim Acta 185:200–215. https://doi.org/10.1007/s00604-018-2687-8
12. Sun NR, Wang JW, Yao JZ, Deng CH (2017) Hydrophilic mesoporous silica materials for highly specific enrichment of N-linked glycopeptide. Anal Chem 89:1764–1771. https://doi.org/10.1021/acs.analchem.6b04054
13. Bibi A, Ju HX (2016) Efficient enrichment of glycopeptides with sulfonic acid-functionalized mesoporous silica. Talanta 161:681–685. https://doi.org/10.1016/j.talanta.2016.09.012
14. Lin Z, Cai ZW (2018) Negative ion laser desorption/ionization time-of-flight mass spectrometric analysis of small molecules by using nanostructured substrate as matrices. Mass Spectrom Rev 37:681–696. https://doi.org/10.1002/mas.21558
15. Kim JI, Parka JM, Noha JY, Hwang SJ, Kang MJ, Pyun JC (2016) Analysis of benzylpenicillin in milk using MALDI-TOF mass spectrometry with top-down synthesized TiO_2 nanowires as the solid matrix. Chemosphere 143:64–70. https://doi.org/10.1016/j.chemosphere.2015.04.002
16. Abdelhamid HN, Lin YH, Wu HF (2017) Thymine chitosan nanomagnets for specific preconcentration of mercury(II) prior to analysis using SELDI-MS. Microchim Acta 184:1517–1527. https://doi.org/10.1007/s00604-017-2125-3
17. Abdelhamid HN, Lin YH, Wu HF (2017) Magnetic nanoparticle modified chitosan for surface enhanced laser desorption/ionization mass spectrometry of surfactants. RSC Adv 7:41585–41592. https://doi.org/10.1039/C7RA05982E
18. Abdelhamid HN, Chen ZY, Wu HF (2017) Surface tuning laser desorption/ionization mass spectrometry (STLDI-MS) for the analysis of small molecules using quantum dots. Anal Bioanal Chem 409:4943–4950. https://doi.org/10.1007/s00216-017-0433-4
19. Sun J, Chen SM, Liu HH, Xiong CQ, Wang JY, Xie XB, Xue JJ, Chen PL, Nie ZX (2016) Fluorographene nanosheets: a new carbon-based matrix for the detection of small molecules by MALDI-TOF MS. RSC Adv 6:99714–99719. https://doi.org/10.1039/c6ra21083j
20. Wang J, Liu Q, Liang Y, Jiang GB (2016) Recent progress in application of carbon nanomaterials in laser desorption/ionization mass spectrometry. Anal Bioanal Chem 408:2861–2873. https://doi.org/10.1007/s00216-015-9255-4
21. Zhao YJ, Tang MM, Liao QB, Li ZM, Li H, Xi K, Tan L, Zhang M, Xu DK, Chen HY (2018) Disposable MoS_2 -arrayed MALDI MS chip for high-throughput and rapid quantification of sulfonamides in multiple real samples. ACS sensors 3:806–814. https://doi.org/10.1021/acssensors.8b00051
22. Lu MH, Yang XQ, Yang YX, Qin P, Wu XR, Cai ZW (2017) Nanomaterials as assisted matrix of laser desorption/ionization time-of-flight mass spectrometry for the analysis of small molecules. Nanomaterials 7:87–107. https://doi.org/10.3390/nano7040087
23. Mandal A, Singha M, Addy PS, Basak A (2019) Laser desorption ionization mass spectrometry: recent progress in matrix-free and label-assisted technique. Mass spectrum Rev 38:3–21. https://doi.org/10.1002/mas.21545
24. Zheng LP, Xing T, Ouyang YH, Wang Y, Wang XY (2019) Core-shell structured MoS_2@mesoporous hollow carbon spheres nanocomposite for supercapacitors applications with enhanced capacitance and energy density. Electrochim Acta 298:630–639. https://doi.org/10.1016/j.electacta.2018.12.126
25. Zhao YJ, Deng GQ, Liu XH, Sun L, Li H, Cheng Q, Xi K, Xu DK (2016) MoS_2/Ag nanohybrid: a novel matrix with synergistic effect for small molecule drugs analysis by negative-ion matrix-assisted

laser desorption/ionization time-of-flight mass spectrometry. Anal Chim Acta 937:87–95. https://doi.org/10.1016/j.aca.2016.06.026
26. Ni LB, Zhao GJ, Yang G, Niu GS, Chen M, Diao GW (2018) Dual core-shell-structured S@C@MnO_2 nanocomposite for highly stable lithium−sulfur batteries. ACS Appl Mater Inter 9:34793–34803. https://doi.org/10.1021/acsami.7b07996
27. Wang Y, Jiao WB, Wang JT, Liu GF, Cao HL, Lu J (2019) Amino–functionalized biomass–derived porous carbons with enhanced aqueous adsorption affinity and sensitivity of sulfonamide antibiotics. Bioresour Technol 277:128–135. https://doi.org/10.1016/j.biortech.2019.01.033
28. Ji YF, Lu JH, Wang L, Jiang MD, Yang Y, Yang PZ, Zhou L, Ferronato C, Chovlon JM (2018) Non-activated peroxymonosulfate oxidation of sulfonamide antibiotics in water: kinetics, mechanisms, and implications for water treatment. Water Res 147:82–90. https://doi.org/10.1016/j.watres.2018.037
29. Liu HL, Sun RX, Feng SY, Wang DX, Liu HZ (2019) Rapid synthesis of a silsesquioxane-based disulfide-linked polymer for selective removal of cationic dyes from aqueous solutions. Chem Eng J 359:436–445. https://doi.org/10.1016/j.cej.2018.11.148
30. Lin LF, Liu YL, Fu S, Qu CH, Li H, Ni J (2019) Inhibition of mitochondrial complex function-the hepatotoxicity mechanism of emodin based on quantitative proteomic analyses. Cell 8:263–279. https://doi.org/10.3390/cells8030263
31. Chen YS, Ding J, He XM, Xu J, Feng YQ (2018) Synthesis of tellurium nanosheet for use in matrix assisted laser desorption/ionization time-of-flight mass spectrometry of small molecules. Microchim Acta 185:368–376. https://doi.org/10.1007/s00604-018-2882-7
32. Yang HM, Su R, Wishnok JS, Liu N, Chen CB, Liu SY, Tannenbaum SR (2019) Magnetic silica nanoparticles for use in matrix-assisted laser desorption ionization mass spectrometry of labile biomolecules such as oligosaccharides, amino acids, peptides and nucleosides. Microchim Acta 186:104–112. https://doi.org/10.1007/s00604-018-3208-5
33. Xie JF, Zhang H, Li S, Wang RX, Sun X, Zhou M, Zhou JF, Lou XW, Xie Y (2013) Defect-rich MoS_2 ultrathin nanosheets with additional active edge sites for enhanced electerocatalytic hydrogen evolution. Adv mater 25: 5807-5813. 10.1002./adma.201302685

Publisher's note Springer Nature remains neutral with regard to jurisdictional claims in published maps and institutional affiliations.